Journal of Colloid and Interface Science 585 (2021) 386–399

Contents lists available at ScienceDirect

Journal of Colloid and Interface Science

journal homepage: www.elsevier.com/locate/jcis

Regular Article

Toward green flotation: Interaction of a sophorolipid biosurfactant with a copper sulfide

Priyanka Dhar [a], Hakon Havskjold [a], Maria Thornhill [a], Sophie Roelants [b,c], Wim Soetaert [b,c], Hanumantha Rao Kota [a,*], Irina Chernyshova [a,*]

[a] Department of Geoscience and Petroleum, Norwegian University of Science and Technology (NTNU), NO-7031 Trondheim, Norway
[b] Bio Base Europe Pilot Plant, Rodenhuizekaai 1, 9042 Ghent, Belgium
[c] Centre for Industrial Biotechnology and Biocatalysis (InBio.be), Department of Biotechnology (BW25), Faculty of Bioscience Engineering, Ghent University, Coupure Links 653, 9000 Ghent, Belgium

HIGHLIGHTS

- Acidic sophorolipid (ASL) has unconventional pH-dependent interfacial properties.
- At the air-water interface, Π-shaped ASL molecules are linked via COOH/COO^- groups.
- ASL has strong metal-leaching properties due to the formation of ring chelates.
- ASL-adsorbed $Cu_{1.94}S$ is hydrophilic at pH < 6.5 and hydrophobic at pH ≥ 7.
- Hydrophobicity at pH ≥ 7 is caused by precipitation of Cu(II)-ASL complexes.
- Adsorption of ASL at pH ≥ 7 is explained by the dissolution-precipitation mechanism.

GRAPHICAL ABSTRACT

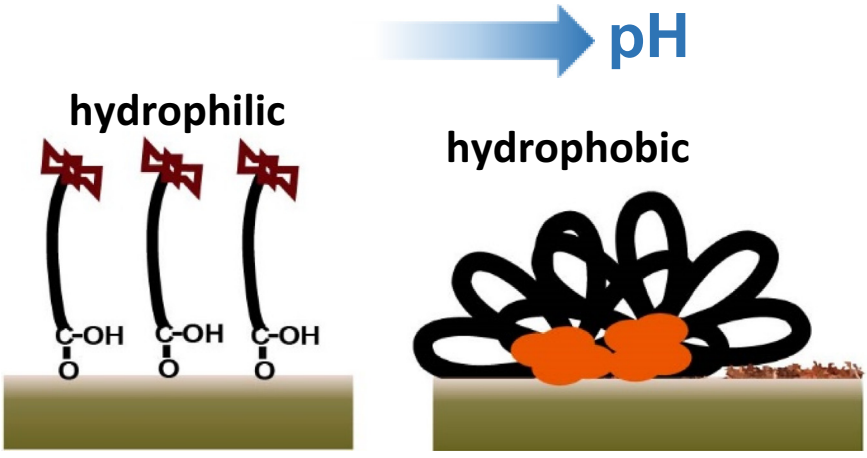

ARTICLE INFO

Article history:
Received 22 June 2020
Revised 15 November 2020
Accepted 23 November 2020
Available online 26 November 2020

Keywords:
Copper sulfide
Glycolipid
Bipolar surfactant
Foam flotation
Metal extraction
FTIR

ABSTRACT

The United Nations' Sustainable Development Goals have sparked growing interest in biosurfactants from many surfactant-loaded industries including those utilizing froth flotation for mineral separation. However, the interaction of biosurfactants with mineral surfaces is currently poorly understood. We bridge this gap by studying adsorption of a yeast-derived bola acidic sophorolipid (ASL) biosurfactant on djurleite ($Cu_{1.94}S$). The methods used include Hallimond flotation, contact angle, adsorption isotherm, zeta potential, leaching measurements, and X-ray photoelectron spectroscopy (XPS). To facilitate the interpretation of the adsorption results, we characterize the activity of ASL at the air-water interface and measure its critical micelle concentration (CMC) at different pH using static surface tension. We find ASL to be a multifunctional surfactant with an unusual, pH-sensitive interfacial behavior. At the air-water interface, ASL is most active at pH 8, while its CMC goes through minimum as low as 40 μM at pH 7. The surfactant adsorption at the djurleite-water interface makes the sulfide surface hydrophilic at acidic pH and hydrophobic at neutral and basic pH. In addition, ASL has strong affinity to copper sulfide and demonstrates metal leaching properties. Finally, ASL demonstrates detergency properties. We offer a

* Corresponding authors.
E-mail addresses: hanumantha.rao.kota@ntnu.no (H.R. Kota), irina.chernyshova@ntnu.no (I. Chernyshova).

https://doi.org/10.1016/j.jcis.2020.11.079

mechanistic interpretation of these findings. Our results provide a basis for the application of acidic glycolipids in froth flotation and have implications for their application in ion separation using hydrometallurgical routes, as well as for the chemical stability of metal sulfides in environmental systems.

1. Introduction

Microbial biosurfactants (100% bio-based surfactants produced by microorganisms) are increasingly being introduced into many industries including home and personal care, cosmetics, agriculture, food, environmental remediation, and pharmaceutical sectors. Their advantages include environmental compatibility, biodegradability, relatively low cytotoxicity, combined with beneficial functional properties such as detergency, complexing, and anti-microbial activity. From the scaling-up view-point, some biosurfactants are already produced quite efficiently, using yeasts through highly productive and eco-friendly bioprocess routes from renewable resources (biomass). These resources can be primary (e.g., sugar and vegetable oil) and secondary (e.g., side- and waste streams including food waste) generation substrates [1–3]. Substitution of petroleum-derived conventional surfactants by biosurfactants would thus contribute to the establishment of a circular economy.

This work is a part of our research aiming to develop a fundamental knowledge of the interaction of biosurfactants with minerals that would help introduce biosurfactants to froth flotation. Froth flotation is one of the main physico-chemical methods used in the mining industry to extract valuable minerals from ores. It employs a difference in hydrophobicity of mineral particles dispersed in water, which is controlled by selective adsorption of surfactants (called 'collectors'). However, many conventional collectors are petroleum-derived, toxic, hazardous, and not biodegradable. Specifically, xanthates (alkyl dithiocarbonates), the most common thiol collectors of metal sulfides, pose occupational hazards to workers as their decomposition products (CS_2 and OCS) are strong eye and skin irritants, while thiol residuals preclude simple water reuse, and may pollute the environment after disposal of flotation tailings [4–6]. Substitution of conventional toxic collectors by more efficient eco-friendly microbial biosurfactants could make this separation technology environmentally more sustainable [7].

The interaction of biosurfactants with minerals is largely unknown. In contrast to conventional surfactants, biosurfactants feature large headgroups which can be complemented by additional ionic or non-ionic functionalities and branched hydrocarbon chains with *cis* defects. This chemical and structural complexity could translate into new mechanisms of the surfactant interaction with minerals, which are yet to be established.

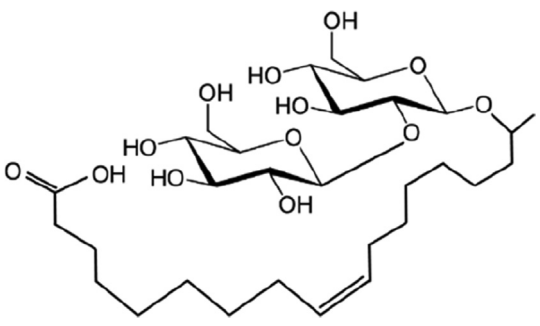

Scheme 1. Acidic C18:1 sophorolipid (ASL).

The present study focuses on the interaction of djurleite $Cu_{1.94}S$ (a copper sulfide from the chalcocite group) with an acidic sophorolipid (ASL) (Scheme 1). This surfactant is known for its detergency [8] and antimicrobial properties [9], and has already been adapted for large-scale production [1–3]. It has an asymmetrical bipolar ('bola') structure with a sophorose headgroup, α-Glc-(1-2)-Glc (diglucose with a β1 → 2′ bond), attached to the C17 carbon of oleic acid C18:1 (where C18:1 refers to an alkyl chain with 18 carbon atoms and 1 mono-unsaturated C=C defect). The hydrophilic sugar group increases solubility of the fatty acid in water and provides additional functionalities for interaction with a mineral surface. Geometric flexibility of the long alkyl chain with a mono-unsaturated defect in its middle can facilitate the formation of a *cis* isomer in which the headgroups interact with one another in a bent structure depicted in Scheme 1, which can underpin novel pH-sensitive self-assembly structures and consequently interfacial properties.

ASL self-assembly has previously been studied in detail mostly in solution [10–14]. As expected, this phenomenon depends strongly on the ionization of the carboxyl group of the surfactant. ASL forms small loosely-packed micelles with an elongated-ellipsoid shape in a broad pH and concentration range [10]. The micelle structure has been found to be rather unusual. Surfactant packing in the ellipsoidal micelles has been described by a coffee-bean model, according to which the micelles' hydrophilic shell is highly inhomogeneous and pH sensitive [14]. Inside the micelles, ASL molecules can be bent or stretched. Sophorose groups constitute the micelle rim, while carboxyl groups are hidden within the sophorose shell [14]. However, due to the small size of the micelles, it is not necessarily true that ASL will self-assemble similarly at the interfaces.

Current knowledge of the interfacial properties of ASL is very limited. ASL adsorption at the air-water interface has only been studied for di-acetylated ASL [15]. Using neutron reflectivity, this study has shown that ASL has a similar affinity for the interface and is similarly distributed there as its lactonic form (a non-ionic derivative in which the carboxylic group is chemically attached to sophorose by esterification). At the same time, the pH-dependence of the adsorption has not been studied, and no clear conclusion has been drawn about the interfacial configuration of ASL.

When deposited on gold, silicon(1 1 1), and TiO_2 (anatase) by dip-coating from concentrated solutions, ASL forms dry deposits with the morphology depending on the solution pH and the substrate [11]. In particular, the deposits are arranged in a homogeneous film on TiO_2 at pH 4, but aggregate at pH 6 and 11. When used as a capping agent in the synthesis of Co and γ-Fe_2O_3 nanoparticles by precipitation, ASL coordinates to the nanoparticles via its carboxylate group while its sophorose group points to the solution, which makes the nanoparticles hydrophilic [16,17]. The hydrophilicity of the sophorose groups of adsorbed ASL has been shown by water contact angle measurements on the ASL molecules self-assembled on Au through their carboxylate headgroups [9]. In contrast, ASL renders chalcopyrite $CuFeS_2$ hydrophobic at neutral and alkaline pH [18], which suggests that both its headgroups interact with the mineral surface. However, the mechanism of the ASL adsorption on the copper sulfide remains unclear as the *ex situ* FTIR spectroscopy does not show any significant

difference in the conformations of the adsorbed and bulk ASL [18], which calls for further studies.

To provide more context, we should mention that there is currently a basic consensus about the interaction of fatty acids with minerals. Fatty acids adsorb on basic metal oxides through a pH-dependent combination of physisorption and chemisorption, which can drive their adsorption even on highly negatively-charged oxide surfaces at alkaline pH [19,20]. In contrast, fatty acids are neither chemisorbed nor physisorbed on clean metal sulfides: Within the hard soft acid base theory, chemisorption is precluded because the carboxylate groups are hard Lewis bases, while the adsorption sites of sulfides such as Cu(I) and Fe(II) are soft and borderline Lewis acids, respectively. Fatty acids cannot physisorb on metal sulfides at neutral and basic pH because the carboxylate groups are repulsed from the negatively-charged sulfide surfaces (their isoelectric point, IEP, is 0–2 [21,22]).

At the same time, there is less clarity about the interaction of saccharide groups with metal sulfides and oxides, especially for molecules that have both saccharide and carboxylate groups. In particular, the adsorption of *n*-dodecyl-β-d-maltoside on solids has been interpreted in terms of hydrogen (H) bonding between the surfactant headgroup and surface hydroxyls [23,24]. In agreement with this model, it has been found that carboxymethyl cellulose interacts with chalcopyrite through the complexation of its carboxymethyl groups with the Fe^{3+} surface sites, rather than through its saccharide groups [25]. In contrast, many studies have argued that saccharide groups can form strong chemical bonds with hydroxylated metal sites of the oxide and sulfide surfaces [26–29], whereas the carboxylate groups have an antagonistic effect on the adsorption [28]. It is worth mentioning that the interaction of polysaccharides with minerals has been studied for several decades due to the capacity of polysaccharides to suppress flotation (such reagents are called 'depressants').

Thus, the interaction of ASL with minerals is a very intriguing but poorly understood phenomenon. To bridge this knowledge gap, we study adsorption of ASL on djurleite using macroscopic methods (zeta potential, adsorption isotherm, leaching, contact angle, and flotation) and XPS. We also gain insight into the self-assembly of ASL at the air-water interface and measure its CMC as a function of pH using surface tension. We find the interfacial properties of ASL to be highly unconventional and propose their mechanistic interpretations.

2. Materials and methods

2.1. Materials

Copper (II) sulfate pentahydrate (99% pure) was acquired from Merck. NaOH (98% pure) and HCl (98.4% pure) were from J.T. Baker. $NaNO_3$ (99.5% pure) was from Sigma Aldrich. Except for flotation, all experiments were conducted in Milli-Q (resistivity of 18.2 M Ω·cm) produced by IQ 7000, Merck group. Deionized water was used in all the Hallimond flotation tests.

Non-acetylated C18:1 ASL ($C_{30}H_{55}O_{13}$, molecular weight 621.7) was synthesized and characterized as described in the Supplementary Material (SM) section. The ASL structure was confirmed using ^{1}H and ^{13}C NMR [17] and FTIR (Fig. S1). Characterization of impurities was performed using HPLC, GC–MS, and ICP-MS (Table S1). The produced ASL sample has a purity of more than 95%. Of the total ASL content, the main component is the C18:1 ASL (90.4%) and 9.6% is made up by other sophorolipids (mainly non-acetylated acidic sophorolipids with C18:0, C18:2 fatty acids incorporated) (Fig. S2 and Table S2). ICP-MS shows that the 1 mM ASL has negligible (<0.3 wt%) admixtures of foreign elements (Table S3). More information is provided in SM.

The djurleite ($Cu_{1.94}S$) mineral used in this study originated from Cornwall (England) (Fig. S3). It was ground by employing a procedure typically used in flotation. Specifically, the mineral was wet ground in a ball mill using 660 g of stainless-steel balls (Ø1.8 mm), followed by sieving to retrieve the −150 + 45 μm size fraction for the Hallimond tube flotation tests. The −10 and −20 μm fractions were prepared by wet grinding of the −45 μm fraction in a Fritsch P6 Pulverizette planetary mono mill at 300 rpm for 5 min. The mill was equipped with a 250 mL stainless steel grinding bowl containing twenty ∅20 mm stainless steel grinding balls. Milled particles were subjected to ultrasound assisted wet screening for 30 min with a 10 or 20 screen, followed by air drying. The −20 μm fraction for the adsorption tests was prepared by dry grinding under the same conditions and wet screened at 20 μm with a RoTap sieve shaker until clear (about 30 min). The undersize fraction was decanted and vacuum filtered on a grade 589/1 Whatman black ribbon filter paper and air dried.

According to the X-ray diffraction (XRD) analysis (Fig. S4), the mineral constitutes 86.4% djurleite ($Cu_{1.94}S$), 6.1% chalcocite (Cu_2S), 5.8% anilite (Cu_7S_4), 1.7% digenite (Cu_9S_5), and 0.08% quartz (SiO_2). In addition to Cu, S, O, C, and Si, XPS shows traces of Ca (Fig. S5).

SEM analysis of the −20 μm fraction shows that the particles are highly polydispersed in the size range from 1 to 30 μm (Fig. S6). They have irregular shapes and rough surfaces, suggesting high concentration of surface defects.

For use as a reference, we prepared a bulk ASL-Cu(II)-SO_4^{2-} precipitate by titrating a 0.01 M solution of Cu(II) sulfate pentahydrate in water with an ASL solution until a pale green sticky hydrophobic precipitate was floating on the solution surface. This precipitate was collected and centrifuged.

2.2. Methods

The phase composition, size, and morphology of djurleite particles were characterized using X-ray diffraction (XRD) and scanning electron microscopy (SEM) as described in SM.

The Brunauer-Emmett-Teller (BET) surface area of djurleite particles was measured using a Micromeritics Tristar 3000 Analyser. Approximately 0.32 g of particles was loaded into a sample tube and evacuated overnight to ~6.7 Pa. Nitrogen was used as the adsorption gas and all adsorption measurements were performed at 77 K. The single-point method gave BET surface areas of 1.1 and 0.82 m^2/g for the −10 and −20 μm djurleite particles, respectively.

Equilibrium surface tension of aqueous surfactant solutions was measured by the Du Nouy's ring method using a computer-controlled surface tension meter (Biolin Scientific, model Sigma702). Glassware was cleaned with chromosulfuric acid and the ring was repeatedly flamed until red-hot and washed with deionized water to ensure the full removal of impurities. The instrument was first calibrated with water (72 ± 2 mN/m). Each reported surface tension data point is an average of 10 measurements in the same solution. Each set of experiments was repeated on two solutions at a particular pH and concentration. Differences between the duplicates were insignificant.

Zeta potential measurements were performed using a DT-310 electroacoustic analyzer (Quantachrome/Dispersion Technologies). The instrument was calibrated using a standard quartz suspension. metal sulfide suspensions were prepared by adding 2 g of the −20 μm size fraction of the metal sulfide particles to 100 mL of 0.01 M $NaNO_3$ or 0.01 M $NaNO_3$ with $1x10^{-5}$ M ASL. The suspensions were magnetically stirred for some time, followed by pH adjustment using HCl or NaOH. Afterwards, suspensions were equilibrated for 1 h and pH was readjusted before measurements. The actual pH was recorded automatically during the

zeta-potential measurements. To assess the accuracy of the zeta-potential results, measurements were performed in triplicate. We report the average values. The maximum standard deviation is 5 mV.

Adsorption tests were conducted at room temperature as follows. A 2-g portion of the −20 μm djurleite was added into 50 mL of an ASL solution at pH 7.0 in a polyethylene bottle. At this point, pH dropped to 6.0–6.5. The pH value was adjusted back to 7.1 ± 0.1 with a NaOH or HCl solution during 2–3 min, and the bottle with the suspension was placed on a shaking table. After 40 min of shaking, the final pH was measured again (almost no change occurred, suggesting that the suspensions were in equilibrium). The supernatant was filtered off using a filter paper (grade 589/1 Whatman black ribbon filters). The exception was the sample conditioned at 1 mM ASL. It was additionally vacuum filtered using a 0.45 μm cellulose nitrate membrane. The reason for this extra step was that the particles were moving across the edge of the wet filter paper due to hydrophobicity (flotation) of the particles. The clear supernatant was divided into two parts. One part was subjected to the total organic carbon (TOC) analysis, while the other was analyzed using ICP-MS. One third of the samples was prepared in duplicate.

TOC analysis was performed using a Combustion Analyzer Apollo 9000 instrument. To remove inorganic carbon, the samples were acidified and saturated with synthetic air. After bubbling with synthetic air, the sample was sent into an incinerator held at 680 °C where carbon was converted to CO_2. The CO_2 detector compares the signal with stored calibration values and calculates the amount of detected CO_2 in ppm. All TOC measurements were conducted in duplicate.

To determine the amount of adsorbed ASL in each adsorption test, we calculated equilibrium ASL concentrations using the calibration line obtained using the initial ASL solutions (Fig. S7). These values were converted into the formal adsorption density (AD) of the adsorbed surfactant as $AD = (C_0\text{-}C_e)V/S$, where C_0 and C_e are the initial and equilibrium concentration of ASL, respectively, V is the solution volume (50 mL), and S is the surface area of the particles (0.82 m^2/g).

Elemental composition of the ASL solutions before and after interaction with djurleite was analyzed using an ICP-HR-MS Element 2 (Thermo) equipped with an auto-sampler - SC2 DX dust covered with a ULPA filter. The ICP-HR-MS measurements were conducted on the blank ASL solutions and the supernatants prepared in the adsorption study, after their digestion using HNO_3. Triplicate measurements were performed on each sample.

Contact angle was extracted from capillary penetration of water into mineral powder beds of the −10 μm size particle fraction. The measurements were conducted using an Attension Sigma 700 apparatus (Biolin Scientific, Germany). The dried powders were packed into a tube (8 ± 0.1 mm diameter) on a filter paper over the frit on its bottom end. The tube was mounted on a probe attached to an electronic balance over a container containing water on a moving stage. Three measurements were performed on each sample to report their average. The maximum relative standard deviation was 2%.

Single mineral flotation tests were performed using a 100-ml Hallimond cell. A 2 g portion of the −150 + 45 μm size fraction of the mineral was conditioned in a solution with a predetermined ASL concentration/pH for 5 min and the suspension was transferred to the flotation cell. Flotation was conducted for 1 min at an air flow rate of 8 mL/min. The concentrate and the tailings were collected, filtered, dried, and weighed to determine the yield of the product. All experiments were performed in triplicate and the relative standard deviation did not exceed 3%.

X-ray photoelectron spectroscopy (XPS) measurements were conducted using a Kratos Axis Ultra DLD spectrometer (Kratos Analytical) with a monochromatized Al X-ray source (hυ = 1486.69 eV) operating at 10 mA and 15 kV (150 W) and a low energy electron beam charge-neutralization flood gun. survey spectra were measured at an electron analyzer pass energy of 80 eV and a resolution of 1 eV. regional spectra were measured at a pass energy of 20 eV and a resolution of 0.1 eV. Each regional and survey spectrum was accumulated for 7–8 min. *The binding energy scale was calibrated by setting the C 1s peak of adventitious sp^3 carbon at 284.6 eV.* Percentage atomic concentrations of the sample surfaces were calculated using CasaXPS software. XPS peaks were fitted with Gaussian–Lorentzian peak profiles (100–80% Gaussian) after subtracting either the Shirley or linear background. S 2p spectra were fitted with doublets with the intensity ratio of 1:2 and splitting of 1.18 eV. MultiPak software was used for reporting the results.

XPS spectra were measured on −20 μm djurleite particles conditioned for 30 min in either water or different ASL solutions. To prepare samples, 2 g of the particles were added into a 100-mL solution at initial pH 8.0 ± 0.1. A 100-mL. At this point, pH dropped to from 7.1 to 6.3 in the solutions with ASL concentration from 1 μM to 1 mM, respectively, but essentially did not change in water. After 30 min of stirring, mineral particles were filtered off using a paper filter and dried under open atmosphere for 2 days. For the XPS measurements, the dry particles were pressed into the freshly-exposed surface of an indium foil (>99% purity, Sigma-Aldrich), and the foil was attached to the XPS holder (Fig. S8). Survey spectra do not reveal In peaks (Fig. S5), which excludes contribution from In/In (hydr)oxide to the XPS spectra. To verify reproducibility, the XPS spectra were measured on two sets of the ASL-conditioned particles prepared independently.

3. Results and discussion

3.1. ASL adsorption at the air-water interface

Before studying adsorption on djurleite, the CMC of ASL was measured as a function of pH and its self-assembly at the air-water interface characterized using static surface tension. CMC has earlier been measured for ASL samples with different purity and at natural pH that has not been reported [1,12,15].

Fig. 1a shows the equilibrium surface tension as a function of ASL concentration in water at pH 4, 7, and 11. At all three pH values, surface tension reaches limiting values of 38–40 $mN{\cdot}m^{-1}$ (Table 1), which are in good agreement with reported values [1,12,15]. CMC extracted from these plots is 0.4 mM, 40 μM, and 0.10 mM at pH 4, 7, and 11, respectively (Fig. S9). The minimum surface area per surfactant, A_{min}, also goes through the minimum at pH 7 (Table 1) (the A_{min} calculation is described in SM). In addition, the pH dependence of the surface tension at ASL concentrations of 2.1 and 13 μM (which are well below CMC) demonstrates a pronounced minimum at pH around 8 (Fig. 1b). These results indicate that ASL self-assembly is most effective in water and at the air-water interface at pH 7–8.

The pH dependence of the surface tension created by ASL is remarkably different from that reported for other surfactants with a large O-rich headgroup complemented by a carboxyl group. For example, the surface tension of rhamnolipids decreases with decreasing pH, with a plateau at pH from 10 to 4 [8,30]. Nonaoxyethylene oleylether carboxylic acid, $R\text{-}O(CH_2CH_2O\text{–})_nCH_2COOH$, R = C16/C18, n = 9) demonstrates a monotonic decrease in the surface tension with decreasing pH [31]. This effect has been explained by a denser packing of the surfactants with decreasing electrostatic repulsion between their carboxylate groups.

In contrast, the pH dependence of the surface tension of ASL is similar to that of fatty acids, which also have a minimum at pH 7.5–9.0 [32]. This minimum is commonly interpreted in terms of

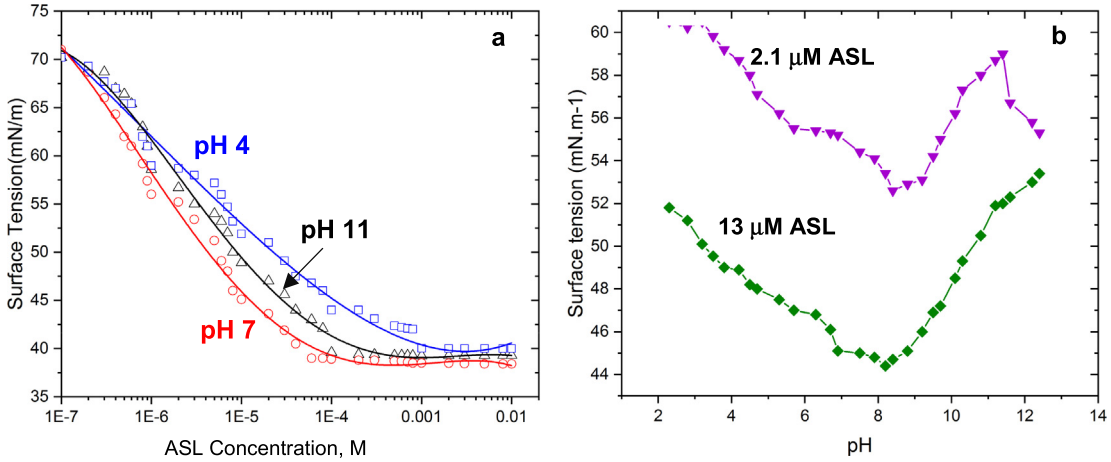

Fig. 1. Surface tension of ASL as a function of (a) concentration at pH 4, 7, and 11 and (b) pH at ASL concentrations 2.1 and 13 μM. Differences between duplicates were insignificant.

Table 1
Limiting surface tension, critical micelle concentration (CMC), and minimum surface area (A_{min}) of ASL at the air-water interface at different pH values.

Properties at air-water interface	pH 4	pH 7	pH 11
Surface tension at CMC (mN/m)	40	38.5	39
A_{min} (molecule/Å^2)	86	75	150
CMC (mM)	0.4	0.04	0.1

the premicellar activity of fatty acids in the bulk solution. Specifically, it coincides with maximum concentration of the ion-molecular dimers $(RCOO)_2H^-$ of a fatty acid in solution [33]. When these dimers are self-assembled at the interface, the lateral repulsion between their carboxylate groups is screened by the intermingled neutral carboxylic groups, which makes the surfactant packing denser. In addition, the carboxylate and carboxyl headgroups in the ion-molecular pair are strongly attracted to one another by the ion-dipole (or acid-base) interaction, which further increases the cohesive intermolecular forces between the adsorbed molecules as compared to the purely ionic and molecular counterparts. This attractive interaction manifests itself by an increase in apparent pK_a of fatty acids from 4.8 to 5.0 in a monomer to 7.5–9.5 in the interfacial or solution aggregates [34,35].

The fatty-acid-like pH dependence of the surface tension of ASL suggests that the carboxylic groups in the ASL monolayer contact water and directly interact with one another as in a monolayer of fatty acids. This is possible if ASL adopts a Π-shape at the interface where both the carboxylic and sophorose headgroups point to water, the hydrophobic alkyl chain protrudes towards air, while the carboxyl/carboxylate groups of two neighboring Π-shapes contact one another forming a dimer (Scheme 2). The Π-shape of adsorbed ASL agrees with the fact that A_{min} of 75 Å^2/molecule occupied by ASL at pH 7 is only slightly above 72 ± 1 Å^2/molecule occupied by diacetyl lactonic sophorolipid C18:1 (in which the carboxylic and sophorose headgroups are chemically bonded) [15]. The Π-shape at the air-water interface has earlier been reported for a symmetric bola amphiphile [36]. We are the first to report it for an asymmetric bola surfactant. Since CMC of ASL also goes through the minimum in this pH range (Table 1), it is likely that carboxyl groups of ASL are also paired in micelles, which is feasible in the coffee-bean arrangement of the bent ASL molecules [14]. It would be instructive to verify the above conclusions using spectroscopic and molecular dynamics modelling methods.

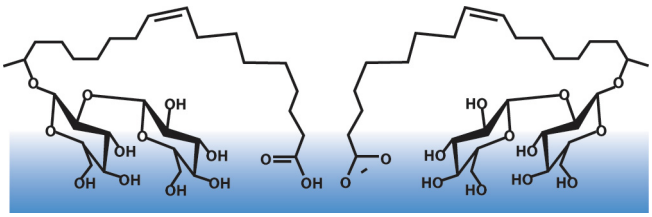

Scheme 2. Postulated self-assembly of ASL at the air-water-interface at pH 8 via dimers in which the molecules adopt a Π-shape and interact with one another via their carboxyl/carboxylate groups.

Our model (Scheme 2) explains the decrease in the surface activity of ASL at pH above 8 as in the case of fatty acids, by an increase in the relative interfacial concentration of carboxylate groups, which makes their repulsion unscreened. However, the analogy with fatty acids runs short in the pH range below 8. For fatty acids, the decrease in the surface activity in this pH range has been explained by the precipitation of neutral molecules or their partitioning to the oil droplets at the air-water interface due to the protonation-driven drop in their solubility [34,35]. This hardly happens for ASL at 2.1 and 13 μM because of its relatively high solubility at acidic pH, at least 10 mM at pH 4 (Fig. 1a). Instead, protonation of the carboxylate groups can lead to a decrease in the surface activity of ASL through weakening the intra- and inter-molecular attraction between the headgroups of the self-assembled Π-shaped molecules, which causes their lateral dilation and increases the spacing between them, respectively.

In summary, we find that ASL acquires at the air-water interface a bent Π-shape, while the carboxylic/carboxylate headgroups of two neighboring molecules interact with one another (Scheme 2). This self-assembly pattern explains the increase in the surface activity of ASL at pH 8.The ability of ASL to adopt Π-shape suggests that both its headgroups are sterically available for chelating metal ions, which is behind its leaching activity and strong affinity to the djurleite surface (see below).

3.2. Macroscopic characterization of the ASL adsorption on djurleite

3.2.1. Zeta potential

In the absence of ASL, the sulfide surface is progressively negatively charged with increasing pH (Figs. 2 and S10). Its IEP (the pH value where zeta potential changes sign) is around pH 4, in good agreement with the reported value of 4.4 [21]. An IEP around 4 suggests that the sulfide surface is in a medium oxidation state.

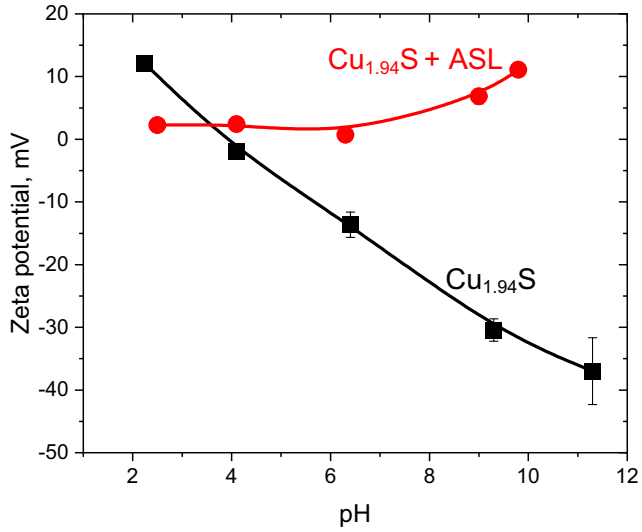

Fig. 2. Effect of pH on zeta potential of −20 μm djurleite established in 1 h in 0.01 M $NaNO_3$ (dashed line) in the absence and (solid line) in the presence of 10 μM ASL. The maximum standard deviation of zeta potential in triplicate measurements (n = 3) is 5 mV.

For comparison, the IEP of non-oxidized sulfides such as covellite (CuS) and chalcopyrite is in the pH range of 0–2 [21,22]. Surface oxides increase IEP up to 9 and can generate a secondary IEP [37,38].

In the presence of 10 μM ASL, which is below CMC, zeta potential becomes zero at acidic pH and, surprisingly, increasingly positive at pH above 7 (Fig. 2). This picture is reproduced in the absence of a background electrolyte at a shorter equilibration time (Fig. S10). In contrast, an acidic C18:1 glycolipid (its sugar headgroup includes one glucose ring) and an alcoholic C18:1 glycolipid (which has –OH instead of –COOH at the other end of its C18:1 chain) screen the zeta potential of chalcopyrite in the whole pH range [18].

The disappearance of the zeta potential at acidic pH (Fig. 2) suggests that ASL is adsorbed in this pH range in the molecular form. Adsorption of neutral species typically screens zeta potential because is moves the shear plane farther from the Stern plane.

The increase in the positive zeta potential of djurleite in the presence of ASL at alkaline pH (Fig. 2) is unusual given that anionic surfactants and carboxymethyl cellulose typically charge mineral surfaces negatively [18,25,38,39]. We explain this anomaly by surface precipitation of Cu(II)-ASL complexes that are formed due to the strong metal-leaching/dissolution activity of ASL. This explanation is based on a similar increase in the positive zeta potential of bulk ASL-Cu(II)-SO_4^{2-} precipitates synthesized by titrating a Cu(II) sulfate solution with an ASL solution (Fig. S11), combined with the other results of this study (see below). The activation of the dissolution-precipitation mechanism at neutral and alkaline pH can be linked to the fact that saccharides interact only with hydroxylated cations [23,24,26–29]. As a result, ASL is capable of leaching Cu(II) cations (which is followed by precipitation of the Cu(II)-ASL complexes) only when hydroxylated Cu(II) cations become available at the sulfide surface.

The increase in the positive zeta potential suggests that the ASL-Cu(II) precipitates attract more Na^+ cations (the only positively-charged species at alkaline pH). These cations penetrate into the Stern layer of the precipitates, making the zeta potential positive. The co-adsorption of Na^+ with ASL is observed by XPS (Fig. S5), while the overcompensation of surface charge by counter-ions is a well-known phenomenon [40]. However, it remains unclear which force/interaction drives the Na^+ overcompensation. Given its absence in the case of adsorbed and precipitated acidic glucolipid and alcoholic glucoside [18], this effect is likely to be caused by features of the microscopic structure of the ASL-Cu(II) precipitates, e.g., their membrane properties and heterogeneity. Further studies are required to gain insight into this.

To summarize, ASL screens charge of the mineral surface at acidic pH and renders it positively charged at basic pH. The positive charge can be explained by the surface deposition of Cu(II)-ASL precipitates.

3.2.2. Adsorption isotherm

The ASL adsorption isotherm was measured on −20 μm djurleite particles in room temperature water at pH 7. Since we used the TOC method rather than an analytical method specific to ASL to quantify the depletion of ASL upon its adsorption, we called the measured adsorption density "formal adsorption density". As seen from Fig. 3a, this characteristic is negative at ASL concentrations below ca. 50 μM (below CMC). The negative values can be explained by the detergency properties of the surfactant: It solubilizes the adventitious carbon contaminations introduced during the particle preparation (grinding, sieving, and handling), which increases the TOC amount in the solution as compared to the initial ASL solution. This explanation is supported by a high concentration of adventitious carbon on the sulfide surface washed with pure water (see the XPS section below).

With increasing ASL concentration above CMC, the formal adsorption density of ASL goes through the maximum of 3.8 μmole/m^2 at 0.5 mM and then decreases to 2.5 μmole/m^2 at 1 mM (Fig. 3a). The maximum value is by a factor of 1.7 higher than 2.2 μmole/m^2 that ASL occupies at the air-water interface at pH 7 (calculated from A_{min} of 75 $Å^2$/molecule). The real factor is expected to be higher due to the negative contribution of the adventitious carbon to the formal adsorption density value. It follows that at concentrations in the 0.5–1.0 mM range ASL is adsorbed at a larger amount than that of a formal monolayer.

3.3. Leaching properties of ASL

The ICP-MS analysis of the supernatants of djurleite dispersions reveals that ASL has strong leaching properties. As seen from Fig. 3b, increasing ASL concentration at pH 7 increases the concentration of dissolved Cu. At 1 mM ASL, the concentration of Cu is 0.14 mM. At ASL concentrations above 50 μM and higher, which are above CMC of 40 μM, the ASL:Cu solution ratio of 7 ± 1 is constant (except for the 0.5-mM point), suggesting that the dissolved copper cations are associated with ASL micelles. Apart from Cu, ASL leaches out metallic impurities such as Ca, Mg, Al, and Fe (the latter three are not shown in Fig. 3b as their concentrations are below 0.1 ppm).

The observed leaching activity of ASL is in line with the reported strong complexation/ chelating properties of ASL toward adsorbed heavy metals including Cu^{2+} [41–43]. In particular, it has been proposed that ASL forms complexes with adsorbed cations, followed by the detachment of these complexes into the solution through their association with the surfactant micelles [42]. For comparison, oleate inhibits dissolution of Cu(I) sulfide [44]. Hence, even though the carboxylate group of ASL participates in the complexation (see section *XPS study*), the main role is played by the sophorose group.

In addition to metals, ASL solubilizes sulfur (Fig. 3b, S12). Based on XPS results (below), this sulfur can come from surface oxidation products such as hydrophobic elemental sulfur and polysulfides. Solubilization of elemental sulfur by ionic surfactants is a well-known phenomenon [45]. It roots to their detergency properties.

The increase in metal leaching at concentrations higher than 0.5 mM, when a formal ASL multilayer is formed (Fig. 3b) indicates that ASL adsorption is highly non-uniform and does not fully

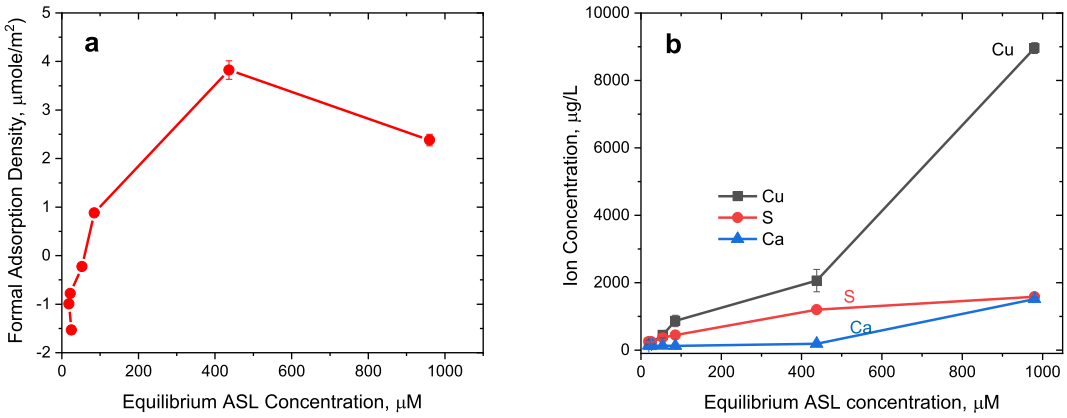

Fig. 3. Effect of ASL concentration on (a) ASL adsorption on and (b) ion leaching by −20 μm djurleite in water at pH 7 during 40 min. The TOC and ICP-MS measurements in (a) and (b), respectively, were conducted on the same solutions. The adsorption density points present the mean values with the maximum error bar of ± 5% obtained in duplicate measurements. The maximum standard deviation of ion concentrations in triplicate measurements (n = 3) is 15%.

passivate the mineral surface. Non-uniformity of the ASL surface coverage can be caused by high heterogeneity of the particle surface and polydispersity of the particle size (Fig. S6).

In combination with the adsorption isotherm, the leaching results suggest that ASL is adsorbed as precipitates of Cu(II)-ASL complexes, in agreement with the conclusion derived from the zeta potential data.

3.3.1. Effect of ASL adsorption on hydrophobicity of djurleite

Contact angle and flotation were used to characterize the effect of ASL on the hydrophobicity of the djurleite surface as a function of ASL concentration and solution pH. This effect is the key property of a surfactant from the flotation view-point. The results confirm the dissolution-precipitation mechanism of the ASL adsorption at neutral and alkaline pH and shed light on the configuration of neutral ASL molecules adsorbed at acidic pH.

Flotation as a function of the ASL concentration at pH 7 shows that djurleite is recovered at a rate of 70% already with 5 μM ASL (Fig. 4). This concentration is 8 times lower than CMC, indicating very high affinity of the surfactant to the sulfide. The corresponding adsorption density of ASL is expected to be well below the theoretical monolayer of 2.2 μmole/m^2 (Fig. 3a). It is likely that under these conditions the adsorbed ASL forms hydrophobic patches. The tendency of ASL to form such patches has been reported earlier [11]. It is known that the formation of one hydrophobic patch is sufficient for the attachment of the particle to an air bubble in the suspension and hence to be floated.

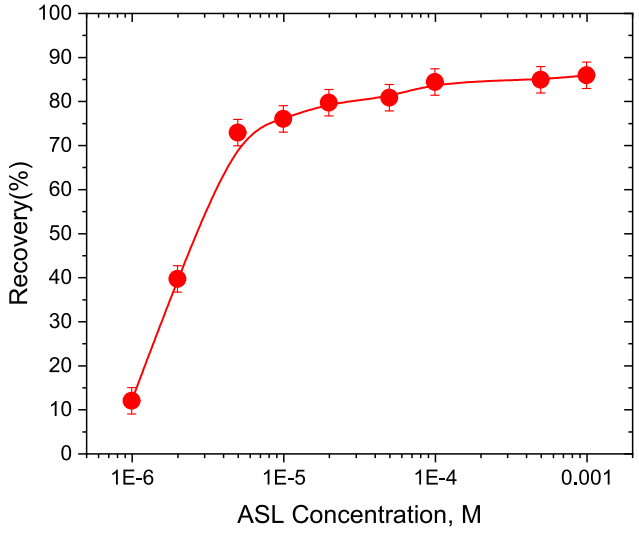

Fig. 4. Hallimond flotation of djurleite as a function of ASL concentration at pH 7. The maximum relative standard deviation of recovery in triplicate independent experiments (n = 3) is 3%.

As concentration increases further to 1 mM (which is well above the CMC), djurleite recovery increases by 15% (Fig. 4). In contrast, an increase in concentration of sodium dodecanoate above its CMC switches the Fe_2O_3 surface from its hydrophobic to hydrophilic state due to the formation of a hydrophilic surfactant bilayer [39]. This difference, along with the TOC and Cu-leaching results (Fig. 3), indicates that ASL is adsorbed at high concentrations at pH 7 in the form of hydrophobic Cu(II)-ASL precipitates, rather than hydrophilic micelles or bilayers.

Below we show that the pH-dependence of hydrophobicity of djurleite (Fig. 5) is consistent with the ASL adsorption at basic and acidic pH via the dissolution-precipitation mechanism and physisorption through the carboxyl group, respectively.

As seen from Fig. 5a, the contact angle measured on the djurleite particles conditioned in ASL-free solutions at acidic pH is ca. 60°. The angle goes further down to ca. 53° at pH 7 and remains the same at basic pH. It follows that the particles are hydrophilic in the whole pH range. The slight increase in the hydrophilicity at basic pH can be explained by the established fact that at pH above 6 Cu(I) sulfides start to get oxidized and are covered by hydrophilic Cu(II) hydroxide precipitates [21,46,47].

The picture changes remarkably in the presence of 10 μM ASL (Fig. 5a): ASL makes the sulfide surface more hydrophilic at acidic pH, as seen from a decrease of the contact angle from 60° to ca. 40°. At pH 6–7, the surface suddenly becomes hydrophobic, which is manifested by a step-wise increase in the contact angle from ca. 40° to 75°. As pH is increased further to pH 12, the contact angle slowly increases to 78°. The same pH dependence is demonstrated by flotation recovery (Fig. 5b). It increases step-wise at pH 6–7 from ca. 20% at acidic pH to ca. 85% at basic pH. This pH dependence is qualitatively different from that typically observed for other anionic surfactants. They typically increase hydrophobicity of minerals at concentrations below CMC in a certain pH range. However, hydrophobicity always goes down at alkaline pH (though there can be a second maximum) due to a decline in the adsorption of anionic surfactants on the negatively charged mineral surfaces [18,20].

The increased hydrophilicity of the sulfide surface at acidic pH suggests that ASL is adsorbed through its carboxyl group while its sophorose groups point toward the solution. This interpretation is supported by a low water contact angle of 48°±2° observed on

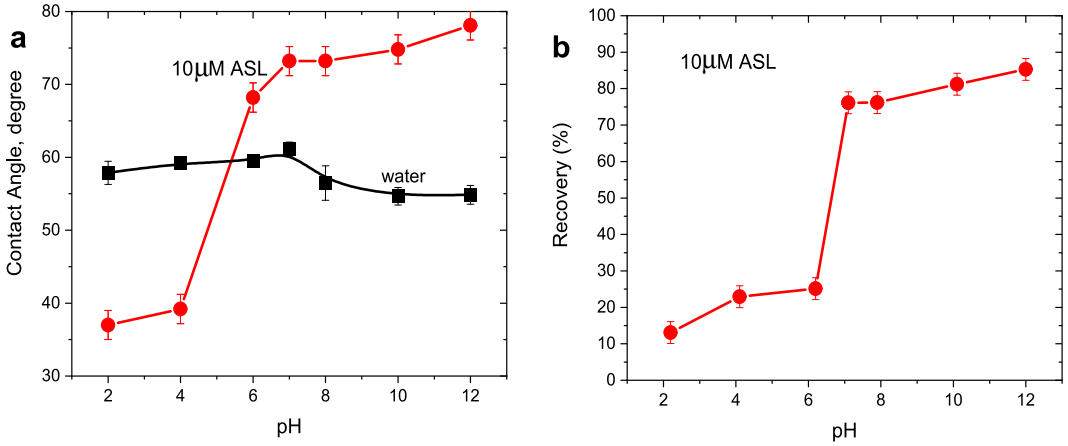

Fig. 5. pH-dependent hydrophobicity of djurleite. It is assessed by measurements of (a) the contact angle on the −10 μm djurleite particles conditioned in water and a 10-μM ASL solution and (b) flotation recovery of −150 + 45 μm djurleite particles. The maximum relative standard deviation of contact angle values in triplicate measurements (n = 3) is 2%.

the sophorose-terminated outer surface of a self-assembled monolayer (SAM) ASL grafted to Au through its carboxylate headgroup [9]. The step-wise increase in the hydrophobicity at neutral pH is consistent with the proposed model of the surface precipitation of Cu(II)-ASL complexes and suggests that these complexes are hydrophobic.

3.4. XPS study of ASL adsorption on djurleite

The molecular structure of the hydrophobic Cu(II)-ASL precipitates was studied using XPS. Before producing these results, we analyze the reference XPS spectra of the water-conditioned mineral, ASL powder, and ASL-Cu(II)-SO_4^{2-} precipitate.

3.4.1. Reference XPS spectra

Djurleite conditioned in water. The survey spectrum of the − 20 μm mineral particles conditioned in water at pH 7 shows that the only extraneous elements on their surface are C, O, and traces of Si and Ca (Fig. S5).

The Cu 2p spectrum of the copper sulfide exhibits the principal Cu $2p_{3/2}$ peak at a binding energy of 932.3 eV typical of Cu(I) in cuprous sulfides and oxides (Fig. 6a) [48,49]. Its pronounced shoulder at ca. 933.7 eV and a strong shake-up satellite at 940–945 eV demonstrate the presence of Cu(II) cations in cupric (hydr)oxides [48,49]. The above results are in agreement with the position and shape of the Cu $L_3M_{4,5}M_{4,5}$ Auger peak at a kinetic energy of 917.7 eV (Fig. S13a) [48,49].

The S 2p spectrum of the water-conditioned djurleite is dominated by the spin-orbit doublet at 161.4 eV typical of the S^{2-} ions of cuprous sulfides (Fig. 6b) [50,51]. An additional weak doublet at ca. 168.2 eV, which accounts for ca. 15% of surface S atoms, can be assigned to the S^{6+} ions of adsorbed SO_4^{2-} groups [50]. These groups are formed on copper sulfides during storage in air [52]. Finally, curve fitting reveals a small doublet at 162.2 eV of Cu-deficient sulfide/polysulfide [53–55]. These species constitute ca. 12% of total surface S atoms. However, their actual surface concentration can be higher and they can be accompanied by elemental sulfur S^0 because the XPS detection of these species is not reliable (they are prone to sublimation under the UHV conditions) [54,55].

The O 1s peak of the water-conditioned djurleite can be fitted with components at 529.6, 530.8, 531.3, 532.2, and 533.1 eV (Fig. 6c). The peaks at 529.6 and 530.8 eV can be assigned to the O atoms in copper oxides (compare with 529.7–529.4 and 530.2–530.3 eV reported for CuO and Cu_2O, respectively [49,56,57]). The peak at 531.3 eV is due to hydroxyl groups. The peak at 532.4 eV can be assigned to the O atoms in sulfate groups and adventitious organic contaminations [49,58,59]. The minor peak at 533.1 eV is consistent with adsorbed water.

The atomic composition (Table 2) shows that the surface of the water-conditioned particles is Cu-enriched: Its Cu/S atomic ratio is 2.6 vs. the stoichiometric ratio of 1.94 of djurleite. In addition, the

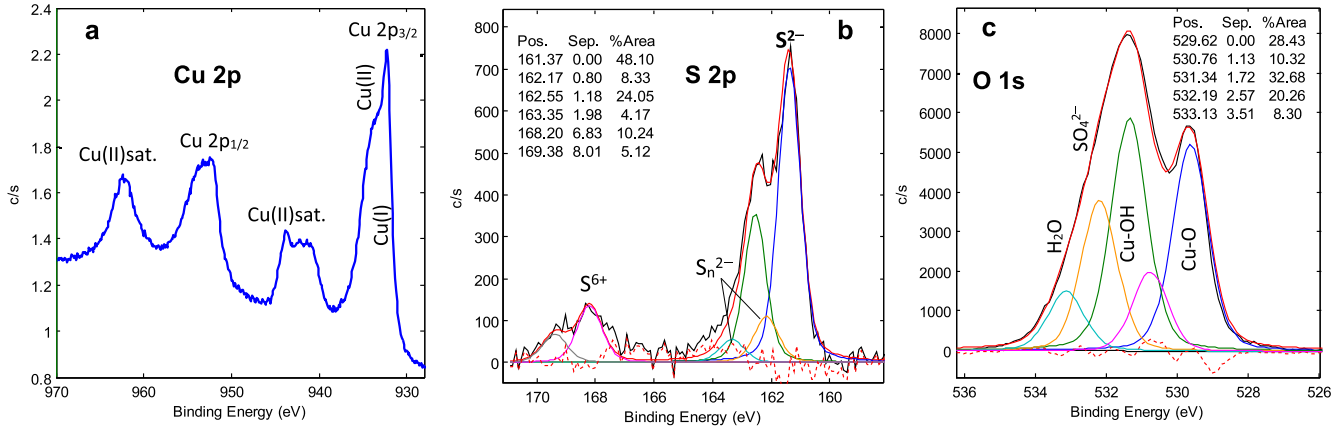

Fig. 6. XPS of djurleite conditioned 30 min in water at pH 7: (a) Cu 2p, (b) S 2p, and (c) O 1s spectra. Sat. = shake-up satellite.

Table 2
Atomic composition of djurleite conditioned in water and ASL solutions at pH 7 as compared to the Cu(II)-ASL-SO_4^{2-} precipitate and ASL powder. It was calculated from regional XPS spectra.

	C, %	% of sophorose C in total C	O, %	S, %	Cu,%	Cu/S
water	44.8	11.1	32.7	6.2	16.4	2.6
1 μM ASL	34.4	11.5	43.6	6.1	15.9	2.6
3 μM ASL	44.0	11.8	32.8	7.2	16.0	2.2
10 μM ASL	52.3	13.5	32.8	7.8	7.0	1.1
1 mM ASL	69.5	36.9	27.5	1.8	1.2	0.7
Cu(II)-ASL-SO_4^{2-}	31.9	36.8	48.5	6.3	6.8	1.1
ASL	71.6	38.3	28.4	0.1	–	–

particles have a high surface concentration (45 at.%) of adventitious carbon (its C 1s spectrum is shown in Fig. S13b)), which explains the negative formal adsorption densities at low ASL concentrations (Fig. 3a).

In summary, the djurleite surface conditioned in water at pH 7 is strongly oxidized. The main oxidation products are Cu(II)/Cu(I) oxides and hydroxides, with admixture of Cu(II)SO_4 and polysulfides, 12–15% each with respect to total S. This surface is copper-enriched and has high concentration of adventitious carbon.

Bulk ASL. The C 1s spectrum of ASL (Fig. 7a) is dominated by two peaks at 284.6 and 286.2 eV assigned to the sp^3 carbon of the hydrocarbon chain and oxidized carbon in the C-OH and C-O-C groups of the sophorose headgroup, respectively [60,61]. Smaller peaks at 287.6 eV and 288.9 eV are due to the O-C-O linkages and the carboxyl (–COOH) group, respectively [60,61]. This peak assignment is supported by a much lower intensity of the 286.2 and 287.6 eV peaks for acidic glucolipid (it has one glucose ring headgroup and one O-C-O linkage) (Fig. S14). The O 1s spectrum of ASL displays a broad peak at 532.6 eV (Fig. S15a) that can be assigned to the overlapped peaks of sophorose and carboxylate/carboxyl groups. The C/O atomic ratio of bulk ASL is 2.5 (Table 2), which is close to the value of 2.3 expected for ASL ($C_{30}H_{55}O_{13}$).

Bulk ASL-Cu(II)-SO_4^{2-} precipitate. The Cu 2p photoelectron and Cu $L_3M_{4,5}M_{4,5}$ Auger spectra of the ASL-Cu(II)-SO_4^{2-} precipitate are characteristic of the Cu(II) cations coordinating SO_4^{2-} groups (Figs. 8 and S15a, respectively). The presence of sulfate groups is confirmed by the S 2p spectrum (Fig. S15c). In addition, the Cu $2p_{3/2}$ peak displays a shoulder at 932.4 eV (Fig. 8) which contributes

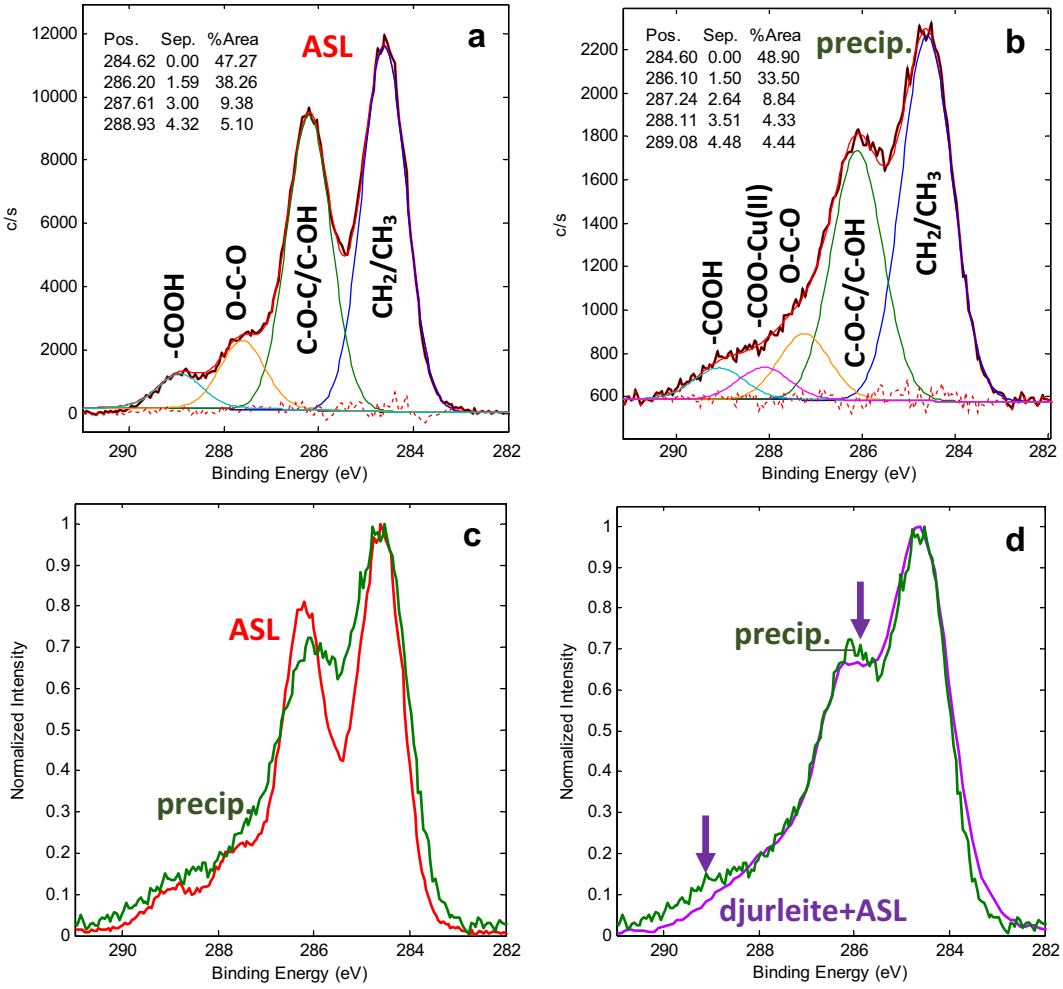

Fig. 7. XPS C 1s spectra: (a) bulk ASL; (b) bulk ASL-Cu(II)-SO_4^{2-} precipitate; (c) their overlap; and (d) bulk ASL-Cu(II)-SO_4^{2-} precipitate and djurleite conditioned with 1 mM ASL. Arrows in (d) show a decrease in the relative intensities of the C-O-C/C-OH and COOH peaks in the ASL adlayer as compared to the precipitate.

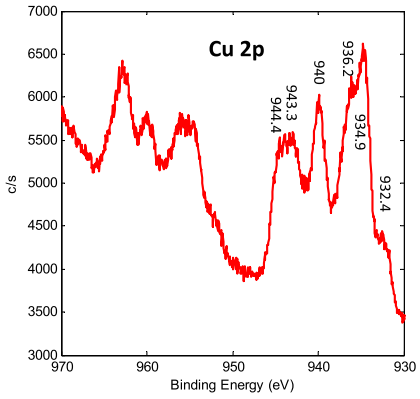

Fig. 8. Cu 2p spectrum of bulk ASL-Cu(II)-SO_4^{2-} precipitate.

14 ± 1% to the total Cu $2p_{3/2}$ peak. This shoulder can be assigned to the Cu(I) cations that can be intrinsic or formed by the reduction of Cu(II) under XPS conditions [62–64]. It is known that the secondary and flood gun electrons can reduce Cu(II) in the presence of organic matter [62].

The O 1s peak of the precipitate at 532.1 eV is shifted from 532.6 eV observed for ASL (Fig. S15a), which can be explained by the contribution of the O atoms of the SO_4^{2-} groups.

As compared to bulk ASL, the precipitate is characterized by broader C 1s peaks (Fig. 7c), which indicates that the chemical environment of its carbon atoms is more inhomogeneous. In addition, the C-O-C/C-OH sophorose peak is shifted from 286.2 eV observed for ASL to 286.05 eV, which suggests that sophorose groups interact with Cu(II). Carbohydrates typically form complexes with transition metal cations through replacement of the proton in the OH groups attached to the anomeric carbon C^1 and C^2 (see [65] and references therein). In parallel, intensity of the C-O-C/C-OH sophorose peak decreases relative to the saturated hydrocarbon peak, pointing out that the sophorose groups in the precipitate are more buried under the hydrocarbon chains than in bulk ASL.

The remaining differences in the C 1s spectra of the precipitate can be described by a shift of the O-C-O peak from 287.6 to 287.2 eV and the appearance of a new peak at 288.1 eV (Fig. 7b). The former effect is in line with the shift of the main sophorose peak in the same direction, both indicating that the sophorose groups interact with Cu(II). The new peak at 288.1 eV can be assigned to the carboxylate groups coordinated by Cu(II). For comparison, the C 1s peak of carboxylic groups of long-chain *n*-alkyl carboxylic acids shifts from 289.0 eV to 288.3 eV when the acids are adsorbed on copper [66]. Similarly, the C 1s peak of carboxylic groups of the carboxylated graphene shifts from 289.0 eV to 288.5 eV upon adsorption of Cu(II) cations [67].

The decrease in the binding energy of the C 1s electrons of carboxyl groups from 288.8 eV to 288.1 eV upon their coordination to Cu(II) can be explained by a more covalent character of the coordination bond as compared to the O-H bond in carboxyls [68]. According to Pauling's valence compensation rule, such a bond would polarize the valence electron density of the coordinated O atom toward the Cu(II) cation. This would weaken the covalent C—O bond that involves this O atom. As a result, the valence electron density on the C atom of this bond would increase, which would downshift the binding energy of its C 1s core-level electron. A similar interpretation has been proposed for a decrease in the binding energy of the C 1s photoelectron of the -C-S_2^- group of xanthate in the Cu(II)-xanthate precipitates as compared to an alkali metal xanthate salt [69].

The inferred interaction of both the headgroups of ASL with Cu(II) is consistent with FTIR spectra of the precipitate (Fig. S16). In addition, the FTIR spectra suggest that the carboxylate group of ASL forms a monodentate complex with Cu(II).

3.4.2. Interaction of djurleite with ASL

The XPS spectra of djurleite particles conditioned at ASL concentrations from 1 μM to 1 mM ASL and pH 6.5–7.0 (Fig. 9) allow us to draw the following four main conclusions.

Firstly, changes in the surface atomic concentrations indicate that the amount of adsorbed ASL increases with ASL concentration (Table 2). As ASL concentration increases, the percentage of C atoms increases, while that of Cu and S decreases, as expected for an organic layer covering the surface. This effect also manifests itself by a gradual lowering of the background in the Cu 2p spectra (Tougaard's effect [70,71]) (Fig. 9a). Alongside, the C 1s spectra show a consistent increase in the relative intensity of the sophorose peak at 286.2 eV (Fig. 9b). The O 1s spectra exhibit the appearance and growth of a new component at 532.6 eV assignable to adsorbed ASL (Fig. 9d). In the limiting case of 1 mM ASL, the O 1s peak is located at 532.6 eV becoming similar to that of bulk ASL (Fig. S15b). The exception is the tail toward lower binding energies which can be assigned to the O-Cu(II) bonds of adsorbed ASL.

Secondly, the XPS spectra demonstrate that ASL strips off copper (hydr)oxides from the sulfide surface. Specifically, the Cu(II) signatures (the high binding-energy shoulders and the shake-up satellites) are gradually suppressed in the Cu 2p spectra as ASL concentration is increased from 1 μM to 1 mM (Fig. 9a). The Cu $L_3M_{4,5}M_{4,5}$ Auger peak acquires features typical of Cu_2S rather than Cu_2O [48,49] (Fig. S15b), while the O 1s spectra show a decrease in the relative intensities of the oxides and hydroxide peaks at 529.6 and 531.3 eV, respectively (Fig. 9d). We should note that the removal of Cu(II) is partially accounted for by the Cu(II) reduction to Cu(I) under the XPS conditions [62–64]. Indeed, Fig. S17 shows that an increase in the number of scans decreases the Cu(II) signatures in the Cu 2p spectrum of the sulfide conditioned at 1 mM ASL. However, the dependence of the Cu(II) features on the ASL concentration along with the leaching results (Fig. 3b) suggests that the main mechanism of the Cu(II) removal is the ASL-promoted dissolution.

Thirdly, as the ASL concentration increases from 0 to 1 mM, the sulfide surface is transformed from metal- to sulfur- rich, as seen from a drop of the Cu/S atomic ratio from 2.6 to 0.7 (Table 2). Accordingly, the S 2p spectra exhibit a steep increase in the metal polysulfide/metal deficient species at 1 mM ASL (Fig. 9c and S18). The formation of the sulfur-rich sulfide surface agrees with the metal-leaching properties of ASL. ASL dissolves the protecting Cu(II) hydroxide coating on the sulfide surface exposing the underlying sulfur-rich surface. This surface is exposed to dissolved oxygen, which causes its further oxidative corrosion. This reaction starts at basic pH presents with dissolution of Cu(II) cations which leads to the formation of a sulfur-rich surface and precipitated Cu(II) hydroxide [21]:

$$Cu_2S + ½\ O_2 + H_2O = CuS + Cu^{II}(OH)_2. \quad (1)$$

In addition, the S 2p spectra demonstrate the SO_4^{2-} doublet at 168.2 eV even after adsorption of more than one ASL monolayer at 1 mM. Since SO_4^{2-} groups are formed by the sulfide oxidation in air [52], their persistence suggests that the ASL adlayer is non-uniform.

The fourth and most important conclusion is that the ASL adlayer can be described as precipitated Cu(II)-ASL complexes. This conclusion follows from the close similarity of the C 1s spectra of the ASL adsorbed at 1 mM and the ASL-Cu(II)-SO_4^{2-} precipitate

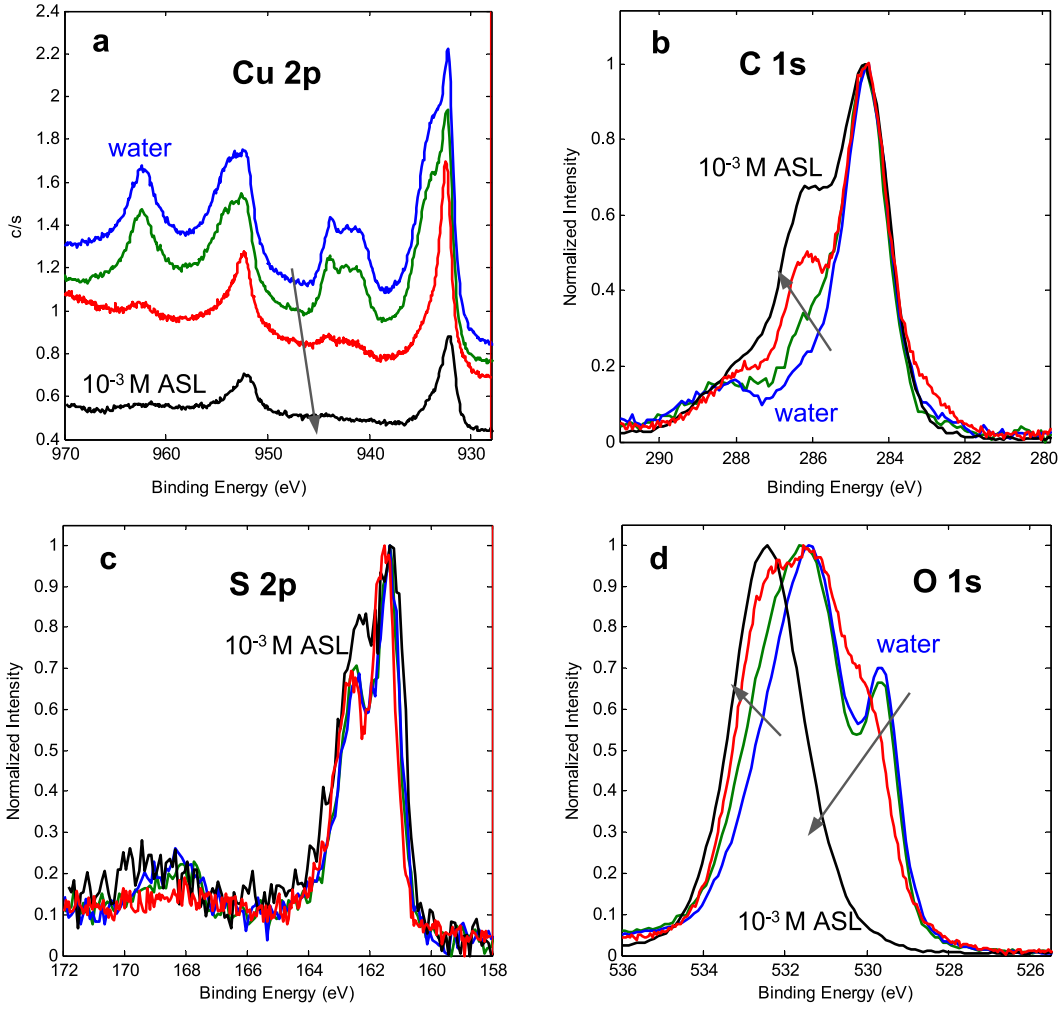

Fig. 9. Effect of ASL concentration in the 0–1-mM range at pH 6.5–7.0 on XPS spectra of djurleite: (a) Cu 2p, (b) C 1s, (c) S 2p, and (d) O 1s regions. The peak intensities in (b)-(d) are normalized by the most intensive peak. Color code: blue = water, green = 1 μM ASL, red = 10 μM ASL, black = 1 mM ASL. The trend corresponding to increasing ASL concentration is shown by arrows. (For interpretation of the references to color in this figure legend, the reader is referred to the web version of this article.)

(Fig. 7d). The exception is that the adlayer is characterized by a lower relative intensity of the sophorose and carboxyl peaks at 286.2 eV and 289.0 eV, respectively. This difference indicates that both the headgroups are shielded more strongly by the hydrocarbon chains in the adlayer as compared to the precipitate.

It has been shown earlier that carboxylate-bridged Cu(II) cations can form multi-ligand polynuclear complexes with saccharide groups at alkaline pH by replacing proton in the acidic OH group attached to the anomeric carbon of the saccharide (see [65] and references therein). This chemical interaction has been proposed to explain spectra of polysaccharides adsorbed on minerals [26–29]. It can be written for the sophorose group of ASL as:

$$\equiv Cu^{II}\text{-}O\text{-}H + HO\text{-}C(sph)\text{-}R\text{-}COO^- \Rightarrow \equiv Cu^{II}\text{-}O\text{-}C(sph)\text{-}R\text{-}COO^- + H_2O, \quad (2)$$

where $\equiv Cu^{II}(OH)_2$ is the hydroxylated surface site and HO-C(sph) denotes the reactive OH group of the sophorose headgroup and R is the C18:1 hydrocarbon chain. Since reaction (2) decreases the local negative charge on the adsorption site, we propose that it facilitates the interaction of the adsorption site with the negatively-charged carboxylate group of ASL through the ligand exchange that results in the formation of a neutral ASL-Cu(II) ring complex:

$$\equiv Cu^{II}\text{-}O\text{-}C(sph)\text{-}R\text{-}COO^- \Rightarrow \equiv Cu^{II}\begin{matrix}O\text{-}C(sph)\\ \diagup\quad R\\ O\text{-}C\\ \diagdown\quad =O\end{matrix} + OH^-. \quad (3)$$

The ring structure of the ASL-Cu(II) complex is supported by monodentate coordination of the carboxylate group of ASL to Cu (II) in the ASL-Cu(II)-SO_4^{2-} precipitate, which follows from FTIR spectra (Fig. S16). Further spectroscopic studies are required to elucidate the chemical structure and organization of the Cu(II)-ASL chelating complexes on the sulfide surface.

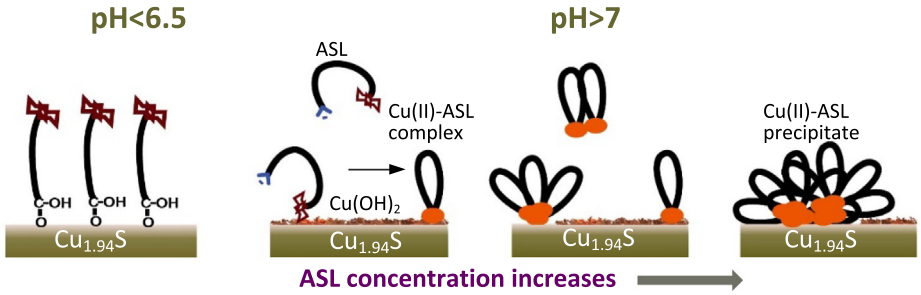

Scheme 3. Proposed mechanisms of the ASL adsorption on djurleite at acidic pH through physisorption and at neutral and basic pH through ligand-promoted dissolution-precipitation.

Combining all the results, we propose the following adsorption mechanism for ASL on djurleite (Scheme 3). At acidic pH, in the absence of adsorbed hydroxyls, ASL is adsorbed in the molecular form through the carboxyl group, while the sophorose group points out rendering the surface hydrophilic. At neutral and basic pH, when the sulfide surface becomes hydroxylated, the adsorption mechanism is switched to the ligand-promoted dissolution-precipitation. It starts with chelating of ASL to a hydroxylated Cu (II) surface site through reactions (2)–(3), followed by dissolution of the Cu(II)-ASL chelating complexes, their aggregation in the electric double layer, and surface precipitation. These precipitates are hydrophobic and hence the surface becomes hydrophobic too.

Surface precipitation of hydrophobic metal-ligand complexes has previously been accepted as one of the main mechanisms of mineral hydrophobization by thiol and hydroxamate collectors [72–76]. It also has been postulated for the adsorption of carboxymethyl cellulose on metal sulfides [25]. Surface oxidation followed by precipitation of copper dodecanoate has been proposed to render a copper surface superhydrophobic in solutions of sodium dodecanoate through conversion of copper dodecanoate precipitate into a superhydrophobic sheet structure [66]. We are the first to report surface precipitation of the metal-surfactant complexes as the adsorption and surface hydrophobization mechanism for glycolipid surfactants.

4. Conclusions

Due to its asymmetric bola structure and the presence of a carboxyl group, ASL demonstrates unconventional pH-dependent interfacial behavior. ASL is most active at the air-water interface at pH 8 because it self-assembles in dimers of the Π-shaped molecules that interact with one another through their carboxyl/carboxylate groups (Scheme 2). The CMC of ASL also depends on pH reaching the minimum value of 40 μM at pH 7, which suggests that ASL self-assembles in micelles in similarly-coupled dimers.

In contrast to conventional (one headgroup-one tail) surfactants at concentrations below CMC, ASL adsorption can make the mineral surface either hydrophilic or hydrophobic depending on pH (Scheme 3). Specifically, ASL renders djurleite hydrophilic at acidic pH and hydrophobic at neutral and basic pH. The hydrophilicity is consistent with the surfactant physisorption through its carboxyl group, while the hydrophobicity is caused by the ligand-promoted dissolution-precipitation mechanism. The latter is underpinned by the strong metal-leaching activity of ASL stemming from its capacity to form ring chelates (3). The Cu(II)-ASL precipitates are responsible for the usual increase in the positive zeta potential of djurleite at alkaline pH.

In addition, ASL demonstrates detergency properties with respect to hydrophobic surface species such as elemental sulfur and adventitious carbon, these properties being synergistic with the adsorption and leaching properties of the surfactant.

The multifunctional interfacial properties of ASL can be of interest for several applications. In particular, the leaching properties can be employed in the hydrometallurgical extraction of metals, while the strong chelating properties can open a door for ASL in ion separation using foam flotation. The pH-controlled role of ASL as either a depressant or collector is very attractive for mineral separation using froth flotation. Toward these practical applications, further studies and tests are required.

CRediT authorship contribution statement

Priyanka Dhar: Investigation, Formal analysis, Writing - original draft. **Hakon Havskjold:** Investigation. **Maria Thornhill:** Supervision, Writing - editing. **Sophie Roelants:** Resources, Writing - editing. **Wim Soetaert:** Resources, Writing - editing. **Hanumantha Rao Kota:** Conceptualization, Supervision, Methodology, Resources. **Irina Chernyshova:** Conceptualization, Supervision, Methodology, Investigation, Validation, Visualization, Writing - original draft, review & editing.

Declaration of Competing Interest

The authors declare that they have no known competing financial interests or personal relationships that could have appeared to influence the work reported in this paper.

Acknowledgements

HH, IVC, and HRK gratefully acknowledge the financial support of the Research Council of Norway (NFR), FRINATEK Project No.: 274691. PD and IVC thank financial support of the Department of Geoscience and Petroleum, NTNU. All the authors thank employees of NTNU for their help with measurements: Laurentius Tijhuis and Torill Sørløkk must be acknowledged for the XRD analysis, Syverin Lierhagen for the ICP-MS measurements, Amin Hossein Zavieh for the XPS measurements, Trine Margrete Hårberg Ness for the TOC measurements, and Ben Snook for the SEM measurements. All the authors greatly appreciate an anonymous reviewer for the very thorough review and the suggestion of substantial improvements.

Appendix A. Supplementary material

Supplementary data to this article can be found online at https://doi.org/10.1016/j.jcis.2020.11.079.

References

[1] S.L.K.W. Roelants, K. Ciesielska, S.L. De Maeseneire, H. Moens, B. Everaert, S. Verweire, Q. Denon, B. Vanlerberghe, I.N.A. Van Bogaert, P. Van Der Meeren, B. Devreese, W. Soetaert, Towards the industrialization of new biosurfactants: Biotechnological opportunities for the lactone esterase gene from Starmerella bombicola, Biotechnol. Bioeng. 113 (3) (2016) 550–559.

[2] L. Van Renterghem, S.L.K.W. Roelants, N. Baccile, K. Uyttersprot, M.C. Taelman, B. Everaert, S. Mincke, S. Ledegen, S. Debrouwer, K. Scholtens, C. Stevens, W. Soetaert, From lab to market: An integrated bioprocess design approach for new-to-nature biosurfactants produced by Starmerella bombicola, Biotechnol. Bioeng. 115 (5) (2018) 1195–1206, https://doi.org/10.1002/bit.26539.
[3] G. Kaur, H. Wang, M.H. To, S.L.K.W. Roelants, W. Soetaert, C.S.K. Lin, Efficient sophorolipids production using food waste, J. Cleaner Prod. 232 (2019) 1–11, https://doi.org/10.1016/j.jclepro.2019.05.326.
[4] Sodium Ethyl Xanthate - Priority Existing Chemical No. 5, Department of Health, Australian Government, 1995.
[5] I. Muzinda, N. Schreithofer, Water quality effects on flotation: Impacts and control of residual xanthates, Miner. Eng. 125 (2018) 34–41.
[6] N.P. Haran, E.R. Boyapati, C. Boontanjai, C. Swaminathan, Kinetics Studies on Effect of Recycled Water on Flotation of Copper Tailings from Benambra Mines, Victoria, Dev. Chem. Eng. Mineral Process. 4 (3-4) (1996) 197–211, https://doi.org/10.1002/apj.5500040305.
[7] G. Jain, H. Havskjold, P. Dhar, H. Ertesvåg, I. Chernyshova, H.R. Kota, Green Foam-Based Methods of Mineral and Ion Separation, in: I. Chernyshova, S. Ponnurangam, Q. Liu (Eds.), Multidisciplinary Advances in Efficient Separation Processes, American Chemical Society, 2020, pp. 265–301.
[8] J. Penfold, R.K. Thomas, H.H. Shen, Adsorption and self-assembly of biosurfactants studied by neutron reflectivity and small angle neutron scattering: glycolipids, lipopeptides and proteins, Soft Matter 8 (3) (2012) 578–591.
[9] C. Valotteau, C. Calers, S. Casale, J. Berton, C.V. Stevens, F. Babonneau, C.-M. Pradier, V. Humblot, N. Baccile, Biocidal Properties of a Glycosylated Surface: Sophorolipids on Au(111), ACS Appl. Mater. Interfaces 7 (32) (2015) 18086–18095.
[10] N. Baccile, M. Selmane, P. Le Griel, S. Prévost, J. Perez, C.V. Stevens, E. Delbeke, S. Zibek, M. Guenther, W. Soetaert, I.N.A. Van Bogaert, S. Roelants, pH-Driven Self-Assembly of Acidic Microbial Glycolipids, Langmuir: ACS J. Surf. Colloids 32 (25) (2016) 6343.
[11] J. Peyre, A. Hamraoui, M. Faustini, V. Humblot, N. Baccile, Surface-induced assembly of sophorolipids, Phys. Chem. Chem. Phys. 19 (23) (2017) 15227–15238, https://doi.org/10.1039/C7CP01339F.
[12] N. Baccile, F. Babonneau, J. Jestin, G. Pehau-Arnaudet, I. Van Bogaert, Unusual, pH-Induced, Self-Assembly Of Sophorolipid Biosurfactants, ACS Nano 6 (6) (2012) 4763–4776, https://doi.org/10.1021/nn204911k.
[13] A.-S. Cuvier, F. Babonneau, J. Berton, C.V. Stevens, G.C. Fadda, G. Péhau-Arnaudet, P. Le Griel, S. Prévost, J. Perez, N. Baccile, Nanoscale Platelet Formation by Monounsaturated and Saturated Sophorolipids under Basic pH Conditions, Chem. Eur. J. 21 (52) (2015) 19265–19277, https://doi.org/10.1002/chem.201502933.
[14] S. Manet, A.-S. Cuvier, C. Valotteau, G.C. Fadda, J. Perez, E. Karakas, S. Abel, N. Baccile, Structure of Bolaamphiphile Sophorolipid Micelles Characterized with SAXS, SANS, and MD Simulations, J. Phys. Chem. B 119 (41) (2015) 13113–13133, https://doi.org/10.1021/acs.jpcb.5b05374.
[15] M. Chen, C. Dong, J. Penfold, R.K. Thomas, T.J.P. Smyth, A. Perfumo, R. Marchant, I.M. Banat, P. Stevenson, A. Parry, I. Tucker, R.A. Campbell, Adsorption of sophorolipid biosurfactants on their own and mixed with sodium dodecyl benzene sulfonate, at the air/water interface, Langmuir: ACS J. Surf. Colloids 27 (14) (2011) 8854.
[16] M. Kasture, S. Singh, P. Patel, P.A. Joy, A.A. Prabhune, C.V. Ramana, B.L.V. Prasad, Multiutility sophorolipids as nanoparticle capping agents: Synthesis of stable and water dispersible Co nanoparticles, Langmuir 23 (23) (2007) 11409–11412.
[17] N. Baccile, R. Noiville, L. Stievano, I.V. Bogaert, Sophorolipids-functionalized iron oxide nanoparticles, Phys. Chem. Chem. Phys. 15 (5) (2013) 1606–1620, https://doi.org/10.1039/C2CP41977G.
[18] P. Dhar, I.V. Chernyshova, M. Thornhill, S. Roelants, W. Soetaert, H.R. Kota, Floatability of Chalcopyrite by Glycolipid Biosurfactants as Compared to Traditional Thiol Surfactants, TSD 56 (5) (2019) 429–435, https://doi.org/10.3139/113.110639.
[19] I.V. Chernyshova, S. Ponnurangam, P. Somasundaran, Adsorption of Fatty Acids on Iron (Hydr)oxides from Aqueous Solutions, Langmuir 27 (16) (2011) 10007–10018, https://doi.org/10.1021/la2017374.
[20] K.B. Quast, A review of hematite flotation using 12-carbon chain collectors, Miner. Eng. 13 (13) (2000) 1361–1376, https://doi.org/10.1016/S0892-6875(00)00119-9.
[21] D. Fullston, D. Fornasiero, J. Ralston, Zeta potential study of the oxidation of copper sulfide minerals, Colloids Surf., A 146 (1) (1999) 113–121.
[22] M.K. Nduna, A.E. Lewis, P. Nortier, A model for the zeta potential of copper sulphide, Colloids Surf., A 441 (2014) 643–652, https://doi.org/10.1016/j.colsurfa.2013.10.024.
[23] L. Zhang, P. Somasundaran, C. Maltesh, Electrolyte Effects on the Surface Tension and Micellization of n-Dodecyl β-d-Maltoside Solutions, Langmuir 12 (10) (1996) 2371–2373.
[24] S. Lu, Y.u. Bian, L. Zhang, P. Somasundaran, pH dependence of adsorption of n-dodecyl-β-d-maltoside on solids, J. Colloid Interface Sci. 316 (2) (2007) 310–316, https://doi.org/10.1016/j.jcis.2007.08.063.
[25] X. Qiu, H. Yang, G. Chen, W. Luo, An Alternative Depressant of Chalcopyrite in Cu–Mo Differential Flotation and Its Interaction Mechanism, Minerals 9 (1) (2019) 1, https://doi.org/10.3390/min9010001.
[26] Q.i. Liu, Y. Zhang, J.S. Laskowski, The adsorption of polysaccharides onto mineral surfaces: an acid/base interaction, Int. J. Miner. Process. 60 (3-4) (2000) 229–245, https://doi.org/10.1016/S0301-7516(00)00018-1.
[27] R.K. Rath, S. Subramanian, T. Pradeep, Surface Chemical Studies on Pyrite in the Presence of Polysaccharide-Based Flotation Depressants, J. Colloid Interface Sci. 229 (1) (2000) 82–91, https://doi.org/10.1006/jcis.2000.6990.
[28] O. Bicak, Z. Ekmekci, D.J. Bradshaw, P.J. Harris, Adsorption of guar gum and CMC on pyrite, Miner. Eng. 20 (10) (2007) 996–1002, https://doi.org/10.1016/j.mineng.2007.03.002.
[29] G.F. Moreira, E.R. Peçanha, M.B.M. Monte, L.S. Leal Filho, F. Stavale, XPS study on the mechanism of starch-hematite surface chemical complexation, Miner. Eng. 110 (2017) 96–103, https://doi.org/10.1016/j.mineng.2017.04.014.
[30] L.-M. Wu, L.u. Lai, Q. Lu, P. Mei, Y.-Q. Wang, L.i. Cheng, Y.i. Liu, Comparative studies on the surface/interface properties and aggregation behavior of mono-rhamnolipid and di-rhamnolipid, Colloids Surf., B 181 (2019) 593–601, https://doi.org/10.1016/j.colsurfb.2019.06.012.
[31] C. Micheau, P. Bauduin, O. Diat, S. Faure, Specific Salt and pH Effects on Foam Film of a pH Sensitive Surfactant, Langmuir 29 (27) (2013) 8472–8481, https://doi.org/10.1021/la400879t.
[32] A. Atrafi, M. Pawlik, Surface tension and gas dispersion properties of fatty acid solutions, Miner. Eng. 85 (2016) 138–147, https://doi.org/10.1016/j.mineng.2015.11.006.
[33] R. Pugh, P. Stenius, Solution chemistry studies and flotation behaviour of apatite, calcite and fluorite minerals with sodium oleate collector, Int. J. Miner. Process. 15 (3) (1985) 193–218, https://doi.org/10.1016/0301-7516(85)90035-3.
[34] J.R. Kanicky, A.F. Poniatowski, N.R. Mehta, D.O. Shah, Cooperativity among Molecules at Interfaces in Relation to Various Technological Processes: Effect of Chain Length on the pKa of Fatty Acid Salt Solutions, Langmuir 16 (1) (2000) 172–177.
[35] J.R. Kanicky, D.O. Shah, Effect of Premicellar Aggregation on the p Ka of Fatty Acid Soap Solutions, Langmuir 19 (6) (2003) 2034–2038, https://doi.org/10.1021/la020672y.
[36] A. Meister, M.J. Weygand, G. Brezesinski, A. Kerth, S. Drescher, B. Dobner, A. Blume, Evidence for a reverse U-shaped conformation of single-chain bolaamphiphiles at the air-water interface, Langmuir: ACS J. Surf. Colloids 23 (11) (2007) 6063.
[37] J. Bebie, M.A.A. Schoonen, M. Fuhrmann, D.R. Strongin, Surface charge development on transition metal sulfides: An electrokinetic study, Geochim. Cosmochim. Acta 62 (4) (1998) 633–642.
[38] R.G. Bhaskar, W. Forsling, Electrokinetic studies on covellite cuprite and tenorite, Bull. Electrochem. 8 (8) (1991) 5.
[39] S. Ponnurangam, I.V. Chernyshova, P. Somasundaran, Rational Design of Interfacial Properties of Ferric (Hydr)oxide Nanoparticles by Adsorption of Fatty Acids from Aqueous Solutions, Langmuir 28 (29) (2012) 10661–10671, https://doi.org/10.1021/la300995g.
[40] D.W. Fuerstenau, Interfacial processes in mineral/water systems, Pure Appl. Chem. 24 (1) (1970) 135–164, https://doi.org/10.1351/pac197024010135.
[41] J. Tang, J.G. He, X.D. Xin, H.Z. Hu, T.T. Liu, Biosurfactants enhanced heavy metals removal from sludge in the electrokinetic treatment, Chem. Eng. J. 334 (2018) 2579–2592.
[42] C.N. Mulligan, R.N. Yong, B.F. Gibbs, Heavy metal removal from sediments by biosurfactants, J. Hazard. Mater. 85 (1) (2001) 111–125.
[43] F. Arab, C.N. Mulligan, An eco-friendly method for heavy metal removal from mine tailings, Environ. Sci. Pollut. Res. 25 (16) (2018) 16202–16216.
[44] P. Nowak, M. Nastawny, I. Kozyra, A. Wegrzynowicz, Controlled adsorption at the surface of copper sulfide minerals - a way to abate the problem of environment contamination by the copper sulfide oxidation products?, Physicochem Probl. Mineral Process. 47 (2011) 131–138.
[45] R. Steudel, G. Holdt, Solubilization of Elemental Sulfur in Water by Cationic and Anionic Surfactants, Angew. Chem., Int. Ed. Engl. 27 (10) (1988) 1358–1359.
[46] G. Fairthorne, D. Fornasiero, J. Ralston, Effect of oxidation on the collectorless flotation of chalcopyrite, Int. J. Miner. Process. 49 (1–2) (1997) 31–48.
[47] D. Fornasiero, J. Ralston, Effect of surface oxide/hydroxide products on the collectorless flotation of copper-activated sphalerite, Int. J. Miner. Process. 78 (4) (2006) 231–237.
[48] P. Velasquez, D. Leinen, J. Pascual, J.R. Ramos-Barrado, R. Cordova, H. Gomez, R. Schrebler, XPS, SEM, EDX and EIS study of an electrochemically modified electrode surface of natural chalcocite (Cu2S), J. Electroanal. Chem. 510 (1–2) (2001) 20–28.
[49] M.C. Biesinger, Advanced analysis of copper X-ray photoelectron spectra, Surf. Interface Anal. 49 (13) (2017) 1325–1334.
[50] M. Kundu, T. Hasegawa, K. Terabe, K. Yamamoto, M. Aono, Structural studies of copper sulfide films: effect of ambient atmosphere, Sci. Technol. Adv. Mater. 9 (3) (2008).
[51] G. Contini, K. Laajalehto, E. Suoninen, A.M. Marabini, 5-Methyl-2-mercaptobenzoxazole Adsorbed onto Chalcocite (Cu2S): An XPS and X-AES Study, J. Colloid Interface Sci. 171 (1) (1995) 234–239.
[52] E.C. Todd, D.M. Sherman, Surface oxidation of chalcocite (Cu2S) under aqueous (pH=2-11) and ambient atmospheric conditions: Mineralogy from Cu L- and OK-edge X-ray absorption spectroscopy, Am. Mineral. 88 (11–12) (2003) 1652–1656.
[53] M. Fantauzzi, B. Elsener, D. Atzei, A. Rigoldi, A. Rossi, Exploiting XPS for the identification of sulfides and polysulfides, RSC Adv. 5 (93) (2015) 75953–75963.
[54] R.S.C. Smart, W.M. Skinner, A.R. Gerson, XPS of sulphide mineral surfaces: metal-deficient, polysulphides, defects and elemental sulphur, Surf. Interface Anal. 28 (1) (1999) 101–105.

[55] V. Nasluzov, A. Shor, A. Romanchenko, Y. Tomashevich, Y. Mikhlin, DFT + U and Low-Temperature XPS Studies of Fe-Depleted Chalcopyrite (CuFeS2) Surfaces: A Focus on Polysulfide Species, J. Phys. Chem. C 123 (34) (2019) 21031–21041.
[56] R.P. Vasquez, Cu_2O by XPS, Surf. Sci. Spectra 5 (257) (1998), https://doi.org/10.1116/1.1247881.
[57] R.P. Vasquez, CuO by XPS, Surf. Sci. Spectra 5 (262) (1998), https://doi.org/10.1116/1.1247882.
[58] R.P. Vasquez, CuSO4 by XPS, Surf. Sci. Spectra 5 (4) (1998) 279–284.
[59] M.C. Biesinger, L.W.M. Lau, A.R. Gerson, R.S.C. Smart, Resolving surface chemical states in XPS analysis of first row transition metals, oxides and hydroxides: Sc, Ti, V, Cu and Zn, Appl. Surf. Sci. 257 (3) (2010) 887–898.
[60] G. Beamson, D.D. Briggs, High Resolution XPS of Organic Polymers – The Scienta ESCA300 Database, Wiley, New York, NY, 1992.
[61] C. Valotteau, S.L.K.V. Roelants, P. Dasaiyan, S. Zibek, M. Günther, W. Soetaert, B. Everaert, C.-M. Pradier, F. Babonneau, N. Baccile, V. Humblot, Antibacterial properties of glycosylated surfaces: variation of the glucosidal moiety and fatty acid conformation of grafted microbial glycolipids, Mol. Syst. Des. Eng. 5 (7) (2020) 1307–1316.
[62] A. Losev, K. Rostov, G. Tyuliev, Electron beam induced reduction of CuO in the presence of a surface carbonaceous layer: an XPS/HREELS study, Surf. Sci. 213 (2) (1989) 564–579.
[63] G.A. Hope, A.N. Buckley, G.K. Parker, A. Numprasanthai, R. Woods, J. McLean, The interaction of n-octanohydroxamate with chrysocolla and oxide copper surfaces, Miner. Eng. 36–38 (2012) 2–11.
[64] C. Magallanes, B.M. Aguirre, G.A. Gonzalez, L.P.M. De Leo, Interaction of aqueous Cu(II) with carboxylic acid and alcohol terminated self assembled monolayers: Surface and interfacial characterization, Surf. Sci. 692 (2020).
[65] C.D. Stewart, H. Arman, H. Bawazir, G.T. Musie, Synthesis, Characterization, and Spectroscopic Investigation of New Iron(III) and Copper(II) Complexes of a Carboxylate Rich Ligand and Their Interaction with Carbohydrates in Aqueous Solution, Inorg. Chem. 53 (20) (2014) 10974–10988.
[66] Z. Zhang, Z. Li, Y. Hu, A. Song, Z. Xue, Y. Li, Z. Sun, X. Kong, W. Xu, S. Zhang, Superhydrophobic copper surface fabricated by one-step immersing method in fatty acid salt aqueous solution for excellent anti-corrosion and oil/water separation properties, Appl. Phys. A 125 (8) (2019) 558.
[67] M. Rosillo-Lopez, C.G. Salzmann, Highly efficient heavy-metal extraction from water with carboxylated graphene nanoflakes, RSC Adv. 8 (20) (2018) 11043–11050.
[68] E.J. Robertson, D.K. Beaman, G.L. Richmond, Designated Drivers: The Differing Roles of Divalent Metal Ions in Surfactant Adsorption at the Oil-Water Interface, Langmuir 29 (50) (2013) 15511–15520.
[69] S.A. Vorobyev, S.V. Saikova, S.B. Erenburg, S.V. Trubina, Y.N. Ivanov, N.G. Maksimov, Y.L. Mikhlin, A comparative study of the structure of copper and lead xanthates, J. Struct. Chem. 58 (6) (2017) 1144–1151.
[70] S. Tougaard, Universality classes of inelastic electron scattering cross-sections, Surf. Interface Anal. 25 (3) (1997) 137–154.
[71] E. Johansson, L. Nyborg, XPS study of carboxylic acid layers on oxidized metals with reference to particulate materials, Surf. Interface Anal. 35 (4) (2003) 375–381.
[72] D.W. Pradip, Fuerstenau, The adsorption of hydroxamate on semi-soluble minerals Part I: Adsorption on barite, Calcite and Bastnaesite, Colloids Surf. 8 (2) (1983) 103–119.
[73] M. Chowdhry, Theoretical study on reactivity of different sulfide collectors and their binding affinity toward Cu(II), Zn(II) and Pb(II) ions, University of Alberta Libraries, 2016.
[74] I.V. Chernyshova, In situ FTIR-spectroelectrochemical study of the anodic processes on a galena (PbS) electrode under open-air conditions in the absence and presence of n-butyl xanthate, Langmuir 18 (18) (2002) 6962–6968.
[75] I.V. Chernyshova, Anodic processes on a galena (PbS) electrode in the presence of n-butyl xanthate studied FTIR-spectroelectrochemically, J. Phys. Chem. B 105 (34) (2001) 8185–8191.
[76] R.S.C. Smart, J. Amarantidis, W.M. Skinner, C.A. Prestidge, L. La Vanier, S.R. Grano, Surface Analytical Studies of Oxidation and Collector Adsorption in Sulfide Mineral Flotation, in: K. Wandelt, S. Thurgate (Eds.), Solid—Liquid Interfaces: Macroscopic Phenomena — Macroscopic Understanding, Springer, Berlin Heidelberg, Berlin, Heidelberg, 2003, pp. 3–62.